PART

III Nuclear interactions

9 The electromagnetic interaction

The electromagnetic interaction, specified by the laws associated with the names of Coulomb, Ampère and Faraday, is well tested over the whole range of energies significant to atomic, nuclear and particle physics. We have already seen that electromagnetic forces are of long range, operating on a macroscopic scale, and that Maxwell's equations, which describe interference and diffraction of light, are relativistically invariant. The quantization of the electromagnetic field must, therefore, be such as to leave these general classical properties unaffected, and this is achieved by the introduction of the massless *photon* as the field quantum.

The photon is a desirable concept, beyond its role in field theory, in order to simplify the description of phenomena such as the emission and absorption of radiation, the photoelectric effect and the Compton effect (Sect. 3.1.4). The field itself may be pictured as in Fig. 2.8, redrawn in Fig. 9.1*a*, in which the exchange of a virtual photon between two charges affects the energy of the system and leads to a force between the charges. In terms of the uncertainty principle argument given in Section 2.2.1, the zero mass of the (real) photon would correspond with a force of infinite range. The virtual photon may also transform itself into a positron–electron pair and these charges separate in the electric field of the original charge creating what is known as a *vacuum polarization.* The strength of the interaction mediated by these virtual processes is characterized by the dimensionless fine-structure constant

$$\alpha = (\mu_0 c^2/4\pi)e^2/\hbar c = \tfrac{1}{137} \tag{9.1}$$

also known as the *electromagnetic coupling constant.*

The virtual radiations just discussed will be re-absorbed by the particle from which they emerge (Fig. 9.1*b*). The theoretical consequences of such processes are profound and have led to the *renormalization* techniques of field theory which are necessary to permit the normal particle-mass to be used meaningfully. Experimentally, these essentially quantum effects account for the Lamb shift of atomic energy levels and for the small anomalous part of the

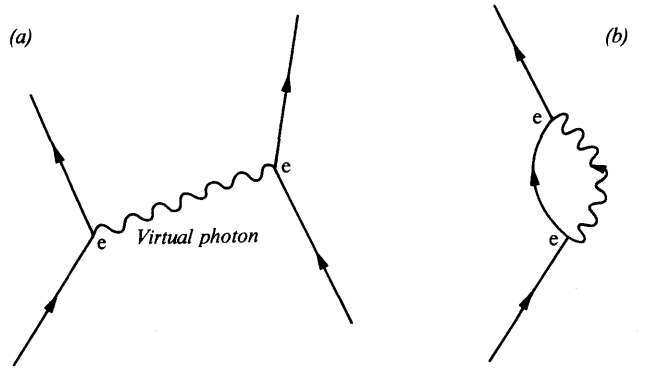

Fig. 9.1 The electromagnetic interaction. (*a*) Electron–electron force, or scattering, described by one-photon exchange. (*b*) Emission and re-absorption of a virtual photon.

magnetic moment of the electron and of the muon. The fact that these quantities are small is due to the actual value of α (eqn (9.1)) and is responsible for the validity of semi-classical calculations of electromagnetic processes in which only *single-photon exchange* between (for instance) a nucleus and a radiation field is considered and the perturbation methods of quantum mechanics are used. These methods will be applied in the present chapter. The smallness of α also makes it useful to classify radiative processes according to the power of α, or of e^2, that enters into the transition probability or interaction cross-section.

Quantum electrodynamics has been exhaustively tested in high-energy electron scattering and bremsstrahlung experiments and in the prediction of the anomalous magnetic moments of the electron and muon. There is no evidence to suggest that these particles behave differently from structureless point charges, and there is no breakdown of the electromagnetic interaction between such charges down to distances of considerably less than the 'classical' radius of the electron, which is $2{\cdot}8 \times 10^{-15}$ m. This interaction is, therefore, likely to be a reliable means of studying nuclear properties, especially the nuclear charge distribution (Sect. 6.2) and the quantum numbers and radiative properties of nuclear levels, with which we will be concerned in the following sections. The role of the static Coulomb interaction in nuclear reactions, in the phenomena of α- and β-decay, in fission and in heavy-ion reactions will be considered in Chapters 10 and 11.

9.1 General properties

9.1.1 Classification and selection rules

The invariance properties of the electromagnetic interaction are listed in Tables 1.1 and 2.3*b*. Classification of radiative processes

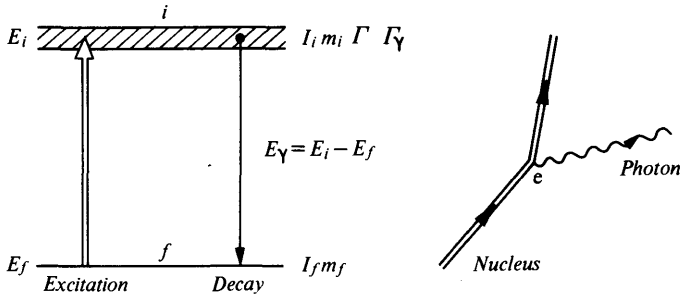

Fig. 9.2 Emission of radiation from a nuclear level of width Γ and radiative width Γ_γ. The sketch at the right is a graph for a first-order decay process. The converse excitation between the levels is also indicated.

such as the nuclear transition shown in Fig. 9.2 is based on the conservation of angular momentum and of parity between the radiating system and the radiation field.

Thus, if an emitted photon transports angular momentum $\boldsymbol{L}$ with respect to the origin, with resolved part $M\hbar$, we have for the level spins (I, m) shown in the figure,

$$\boldsymbol{I}_i = \boldsymbol{L} + \boldsymbol{I}_f \tag{9.2}$$

where in accordance with equation (5.48)

$$|\boldsymbol{L}|^2 = L(L+1)\hbar^2, \qquad |M| \leqslant L$$

From equation (9.2) we then obtain

$$\left.\begin{aligned} I_i + I_f \geqslant L \geqslant |I_i - I_f| \\ m_i = M + m_f \end{aligned}\right\} \tag{9.3}$$

These are the *selection rules* for angular momentum, which limit the *multipolarity* L of the transition, i.e. the number of units of angular momentum $\hbar$ transferred in the radiative process. The meanings of the quantum numbers are shown in the vector diagram, Fig. 9.3*a*.

Despite a small effect due to weak currents (Ch. 10) parity (P) is conserved to a high degree of accuracy in electromagnetic processes and a *parity selection rule* must also be obeyed. The field, however, can be of either even or odd parity for a given multipolarity and the classification of radiative transitions is, therefore, as shown in Table 9.1. The symbols E, M denote fields of *electric* or *magnetic* type respectively and pay due regard to the corresponding classical oscillator.

As indicated in Table 2.3*b* the electromagnetic interaction conserves charge but not isobaric spin. The selection rules for this

TABLE 9.1 Classification of radiative transitions

*Type of radiation**	E1	E2, M1	E3, M2
Name	Electric dipole	Electric quadrupole, magnetic dipole	Electric octupole, magnetic quadrupole
Multipolarity	1	2, 1	3, 2
Parity change in transition	Yes	No	Yes

* Monopole transitions, e.g. E0, do not exist in the radiation field (Sect. 9.1.2).

quantity are

$$\Delta T = 0, \pm 1 \quad \text{(isospin change)}$$
$$\Delta T_z = 0 \quad \text{(charge conservation)}$$

The interaction is invariant under time reversal (T) as is known from experiments on radiative transitions from oriented nuclei, and also under charge conjugation (C) (Table 1.1) since positrons behave electromagnetically in complete analogy to electrons.

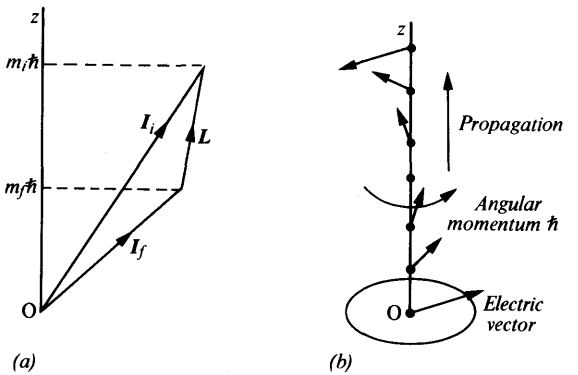

Fig. 9.3 (*a*) Vector diagram for emission of radiation of multipolarity L. (*b*) For propagation along Oz, $M = m_i - m_f = \pm 1$ and radiation is circularly polarized.

9.1.2 The multipole fields (Ref. 9.1)

Because the electromagnetic field of force is a vector field, and the vector potential $\mathbf{A}$ is odd under the parity operation, the photon is assumed to have odd *intrinsic* parity. Moreover, a vector field transforms under rotations like a particle of spin 1 and the spin-parity character of the photon is, therefore, 1^-.

Field vectors are solutions of a wave equation and any arbitrary field specified, for instance, by a vector potential $\mathbf{A}$ can be expanded

in terms of a set of eigenfunctions. For nuclear problems it is convenient (as in the case of the description of a beam of particles, Sect. 1.2.7) to choose eigenfunctions of the angular momentum operators, which will be written $\boldsymbol{L}^2$ and L_z, where for an eigenfunction $\boldsymbol{A}_{LM}$

$$\boldsymbol{L}^2\boldsymbol{A}_{LM} = L(L+1)\hbar^2\boldsymbol{A}_{LM} \tag{9.4a}$$

$$L_z\boldsymbol{A}_{LM} = M\hbar\boldsymbol{A}_{LM} \tag{9.4b}$$

The angular part of such eigenfunctions can be constructed by coupling together the intrinsic spin of the field $\boldsymbol{s}$ with an orbital angular momentum $\boldsymbol{l}$ using the procedures of Appendix 4. For $s = 1$ and a given L, M there are three angular eigenfunctions, known as *vector spherical harmonics*, corresponding with $l = L+1$, $l = L$, and $l = L-1$, and these multiplied by radial functions and added together form a *pure multipole field*, labelled by L, M, for which equations (9.4) hold.

For each multipole field the terms with $l = L \pm 1$ have an orbital parity opposite to that of the term with $l = L$ since the orbital angular functions are the ordinary spherical harmonics Y_l^m. These fields are those of electric and magnetic radiation respectively, and after multiplication by the parity of the photon, give the overall parities shown in Table 9.1. Because of the transverse nature of the electromagnetic field it may be shown (Ref. 9.1) that there is no multipole field in free space for $L = 0$. For nuclear spins $I_i = I_f = 0$, radiation as such is *strictly forbidden*; alternative electromagnetic processes for the $0 \rightarrow 0$ transitions are discussed in Section 9.3.3.

In the present formalism, a photon propagating along the axis Oz may be represented as in Fig. 9.3*b*. There is no component l_z of orbital momentum along the axis and the spin can only have components $\pm\hbar$ if the wave is transverse; these correspond with the two possible signs of circular polarization.

The multipole fields can be used to describe the radiation pattern observed as plane waves at a distance of many wavelengths from the source ($kr \gg 1$, where k is the wavenumber). The angular distribution for a particular multipole indicated by the selection rules is proportional to the square of a vector spherical harmonic. The fields can also be connected with the source densities that give rise to the radiation in the other limiting approximation ($kr \ll 1$). This leads directly to the nuclear matrix element which determines the multipole transition probability, apart from energy-dependent factors.

9.1.3 *The electromagnetic matrix element*

If the coupling between the nuclear current and magnetization distributions is sufficiently weak that second-order effects may be

neglected, the probability per unit time of an electromagnetic transition between the levels i and f shown in Fig. 9.2 is given by time-dependent perturbation theory as

$$T_{if} = (2\pi/\hbar)\,|\langle f|\,H_{em}\,|i\rangle|^2\,\rho(E) \tag{9.5}$$

where $\langle f|\,H_{em}\,|i\rangle = H_{if}$ is the matrix element of the electromagnetic interaction between the initial and final states, and $\rho(E)$ is the phase-space factor giving the number of momentum states per unit energy range at the transition energy in the volume V in which the process is considered to take place. The quantity $\rho(E)$ has the dimensions of $(\text{energy})^{-1}$ and the matrix element itself is an energy. If the wavefunctions occurring in H_{if} are suitably normalized the system volume V will not appear in the final expression for T_{if}. The brackets $\langle\ \rangle$ indicate an integral of the interaction operator between two states and over the volume V in which their wavefunctions exist. Both the specification of the initial and final states and of the interaction Hamiltonian H_{em} depend on the process considered, e.g. electron scattering, Coulomb excitation, internal conversion or absorption and emission of radiation; in the case of elastic electron scattering the transition probability leads to a cross-section which is exactly that predicted by the plane-wave Born approximation (Sect. 6.2).

For purposes of illustration we confine attention to the radiation problem. Although formula (9.5) may be applied directly to an absorption process we shall assume that it is also valid for emission because of time-reversal invariance. The matrix elements are actually complex conjugates in the two cases, and the assumption is justified by a more rigorous calculation using quantum field theory. If the radiation is produced by an oscillating current distribution of density $\boldsymbol{j}$ (A m^{-2}) in the nucleus then the classical interaction energy is

$$H_{em} = \tfrac{1}{2}\int \boldsymbol{j}\,.\,\boldsymbol{A}\,\mathrm{d}V \tag{9.6}$$

where $\boldsymbol{A}$ is the vector potential of the radiation field, which may be written as an outgoing wave

$$\boldsymbol{A} = \boldsymbol{A}_0 \exp i(\boldsymbol{k}\,.\,\boldsymbol{r} - \omega t) \tag{9.7}$$

where $\boldsymbol{k}$ is the wavevector and ω is the frequency. This form of the interaction energy has an immediate application, by analogy, in the theory of weak interactions (Ch. 10) where the energy arises by the interaction of one current with another. Until recently it was thought that only charged currents were effective in such a scheme but, as mentioned in Section 2.2.3, neutral currents are now known also to exist.

In evaluating the matrix element the current density is replaced by the proper quantum operator, which is shown, apart from the ratio e/m, in equation (1.90). This is in the first place applied to a single proton but a sum over all protons in the nucleus may also be taken if necessary. The time factor $e^{-i\omega t}$ disappears, essentially because energy is conserved between the nucleus and the radiation field and we are left with the factor $e^{i\mathbf{k}\cdot\mathbf{r}}$. For radiation of energy ≈ 500 keV the wavelength $\lambda = 2\pi/k$ is 2×10^{-12} m so that kr is a small quantity for an average nucleus and in this *long-wavelength approximation* the exponential may be expanded directly, or the interaction may be expressed as a series of multipole fields, beginning with $L = 1$. In the latter case the radial part of the wavefunction for the multipole L is a spherical Bessel function, which for $kr \ll 1$ has the form

$$j_L(kr) \approx (kr)^L/(2L+1)!! \tag{9.8}$$

where $(2L+1)!! = 1 \,.\, 3 \,.\, 5 \,.\, \cdots \,.\, (2L+1)$.

In either case the interaction finally appears as a set of multipole operators, which for electric radiation have the structure (for a point charge e)

$$er^L Y_L^m(\theta, \phi) \qquad (L \geq 1) \tag{9.9}$$

but for magnetic radiation due to the currents are reduced in value by a factor $\approx v/c$ where v is a typical nucleon velocity in the nucleus, say $v \approx 0{\cdot}1c$. The matrix elements of these operators between the nuclear states $i(I_i, m_i)$ and $f(I_f, m_f)$ are the basic quantities determined by electromagnetic experiments; they are non-zero only for the transitions specified by the selection rules. From (9.8) it may be seen that the intensity of successive multipoles, if allowed by the selection rules, decreases by a factor $\approx (kR)^2$ where R is the nuclear radius, for each increase of 1 in multipolarity. Low multipolarities are, therefore, strongly favoured in nuclear radiation unless the corresponding matrix element is abnormally small.

The treatment so far sketched must be extended to include radiation due to the intrinsic magnetic moments of the nucleons whose state of motion in a nucleus is changing.

9.2 Lifetime-energy relations

9.2.1 General: the Weisskopf formula

For the level i shown in Fig. 9.2 the radiative transition probability T_{if} is the reciprocal of the mean life τ_γ for the emission of radiation and is connected with the radiative width Γ_γ by the equation

$$T_{if} = 1/\tau_\gamma = \Gamma_\gamma/\hbar \tag{9.10}$$

so that

$$\Gamma_\gamma \tau_\gamma = \hbar = 6{\cdot}6 \times 10^{-16}\,\text{eV s} \tag{9.11}$$

It is, of course, just equal to the 'radioactive' decay constant λ of the exponential decay of the state or to $0{\cdot}693/t_{1/2}$ where $t_{1/2}$ is the halflife.

If neither I_i nor I_f is zero, transitions of mixed multipolarity, e.g. M1+E2, may occur between the states. The mixing ratio δ is defined as a ratio of matrix elements but for most purposes it is sufficient to note that

$$\delta^2 = \Gamma_\gamma(L+1)/\Gamma_\gamma(L) \quad \text{e.g.} \quad \Gamma_\gamma(\text{E2})/\Gamma_\gamma(\text{M1}) \tag{9.12}$$

This ratio of partial widths must be obtained using conversion coefficients (Sect. 9.3) or angular correlation experiments (Sect. 9.5) before the individual radiative widths can be extracted from the total radiative width Γ_γ.

A crude estimate of the electric dipole (E1) transition probability may be obtained from the classical formula for the averaged rate of radiation of energy from a simple harmonic oscillator of dipole moment p and angular frequency ω. This is

$$\frac{\overline{\mathrm{d}W}}{\mathrm{d}t} = \left(\frac{\mu_0 c^2}{4\pi}\right)\left(\frac{p^2\omega^4}{3c^3}\right) \tag{9.13}$$

If this radiation is emitted as photons of energy $E_\gamma = \hbar\omega = E_i - E_f$ and if p is replaced by a suitable quantum-mechanical matrix element er_{if}, for the intial and final states shown in Fig. 9.2, then the transition probability for level i is given by

$$T_{if} = \frac{1}{\tau_\gamma} = \frac{1}{\hbar\omega}\left(\frac{\overline{\mathrm{d}W}}{\mathrm{d}t}\right) \propto \left(\frac{E_\gamma}{\hbar c}\right)^3 |r_{if}|^2 \tag{9.14}$$

The transition probability is thus proportional to the transition energy cubed.

Alternatively, and more generally, use may be made of the formula (9.5) for the transition probability, and the multipole expansion of the interaction. The result for multipolarity L is

$$T_{if}(L) = \frac{1}{\tau_\gamma} = \left(\frac{\mu_0 c^2}{4\pi}\right)\frac{8\pi(L+1)}{L[(2L+1)!!]^2}\cdot\frac{1}{\hbar}\left(\frac{E_\gamma}{\hbar c}\right)^{2L+1} B_{if}(L) \tag{9.15}$$

where $B_{if}(L)$, sometimes written $B(L)\downarrow$ to signify an emission process, is the *reduced transition probability* and is the 'internal' factor containing nuclear information. It is essentially the square of the matrix element of the appropriate multipole operator averaged over the $(2I_i+1)$ substates m_i and summed over the accessible substates m_f. For electric transitions $B(L)$ is measured in the units

$e^2\,\mathrm{fm}^{2L}$ and for magnetic transitions in $(\mu_N/c)^2\,\mathrm{fm}^{2L-2}$, where μ_N is the nuclear magneton.

In some experiments such as Coulomb excitation (Sect. 9.4.2) the upward probability $B_{fi}(L)$ or $B(L)\uparrow$ is measured. This has the same matrix element and is thus related to $B(L)\downarrow$ according to the definition by the formula

$$(2I_i+1)B_{if}(L)=(2I_f+1)B_{fi}(L) \tag{9.16}$$

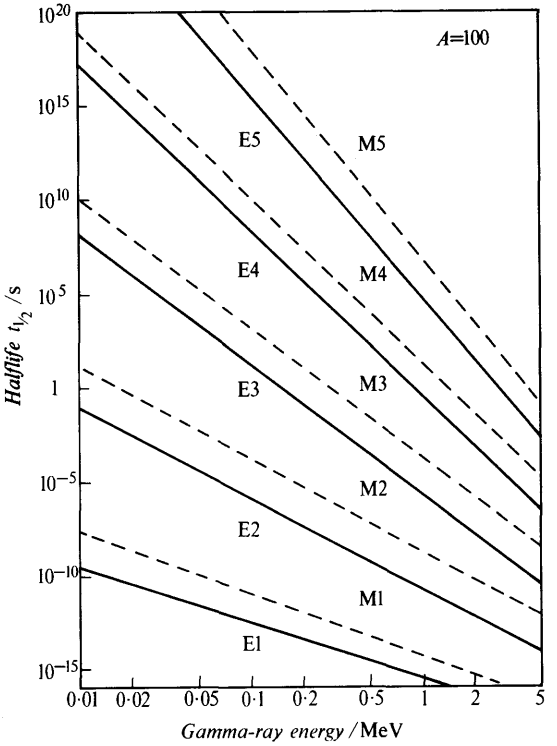

Fig. 9.4 Lifetime–energy relations for γ-radiation according to the single-particle formula of Weisskopf, for a nucleus of mass number $A = 100$.

For practical purposes it is convenient to introduce an estimate of the quantity B_{if}, so that a lifetime–energy relation may be established. The *Weisskopf* formula is based on the *single-particle shell model* and assumes radiation to result from the transition of a single proton from an initial orbital state to a final state of zero orbital angular momentum. The resulting reduced transition probabilities are

$$B(\mathrm{EL})=(e^2/4\pi)(3R^L/L+3)^2 \quad \text{for electric radiation} \tag{9.17a}$$

and

$$B(\mathrm{ML}) = 10(\hbar/m_p cR)^2 B(\mathrm{EL}) \quad \text{for magnetic radiation} \quad (9.17b)$$

where R is of the order of magnitude of the nuclear radius. The factor 10 in $B(\mathrm{ML})$ is introduced to allow for magnetic radiation originating from reorientation of intrinsic spins. The lifetime–energy relations based on these estimates have been very widely used; they are shown in Fig. 9.4 for the particular case of $A = 100$ and it is clearly seen that lifetimes become long as energy decreases and as multipolarity increases. The formulae also give *single-particle radiative widths* directly, e.g.

$$\left.\begin{aligned} \Gamma_\gamma(\mathrm{E1}) &= 0{\cdot}07\, E_\gamma^3 A^{2/3} \\ \Gamma_\gamma(\mathrm{M1}) &= 0{\cdot}021\, E_\gamma^3 \\ \Gamma_\gamma(\mathrm{E2}) &= 4{\cdot}9\times 10^{-8}\, A^{4/3} E_\gamma^5 \end{aligned}\right\} \quad (9.18)$$

where Γ_γ is the radiative width in eV, E_γ the transition energy in MeV and A the mass number of the nucleus. In the individual-particle model radiative widths would be expected to be smaller, because of the sharing of the radiative moment among the several particles of the configuration. The M1 transition probability would vanish in the absence of spin-orbit coupling.

If the nuclear core participates in the radiative process, in-phase motion of particles gives radiative widths which are much larger than the single-particle value (Sect. 8.5).

9.2.2 Nuclear isomerism

Figure 9.4 shows that electromagnetic transitions of high multipolarity and low energy are relatively slow processes. Excited states of nuclei which can only decay by such transitions may, therefore, have a long life. Nuclei excited to these states will differ from unexcited nuclei in their radioactive properties and in their static moments, but not in charge or mass number. Such nuclei are said to be *isomeric* with respect to their ground state.

In nuclei stable against beta decay an isomeric transition is usually accompanied by internal conversion electrons (Sect. 9.3) since the conditions for isomerism are just those for high internal conversion coefficients. The experimentally observed radiation is then often an electron line of low energy decaying with a halflife short compared with that expected for a nuclear beta decay of corresponding energy. The X-rays following the electron emission are characteristic of the radiating atom itself and not of the daughter as in the case of beta decay or electron capture (Ch. 10). There is no clear delimitation of the range of isomeric lifetimes but it is customary to regard them as measurable without special methods, i.e. perhaps $t_{1/2} > 10^{-6}$ s.

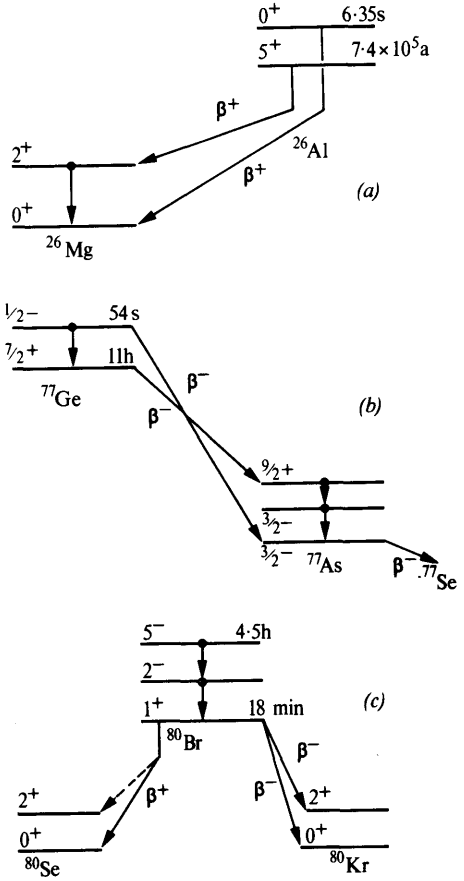

Fig. 9.5 Examples of nuclear isomerism. (*a*) ^{26}Al, in which the isomeric state decays by positron emission and no radiative transition is seen. (*b*) ^{77}Ge in which β- and γ-emission compete in the decay of the $\frac{1}{2}^-$ state. (*c*) ^{80}Br in which the 5^- state decays wholly by radiative transition.

Typical examples of isomeric transitions are shown in Fig. 9.5. Isomers may be produced in all types of nuclear reaction including beta decay, but the yield may be low if the transfer of a large amount of angular momentum is necessary. In such cases it is possible to reach the isomeric level by exciting a higher level of lower spin, from which cascade transitions can take place. The frequency of occurrence of nuclear isomers is plotted as a function of the odd-nucleon number for nuclei of odd A in Fig. 9.6. There is a characteristic grouping just below the major closed shells at Z or $N = 50$ and 82 and a less marked distribution near $N = 126$. These so called 'islands of isomerism' receive an immediate interpretation

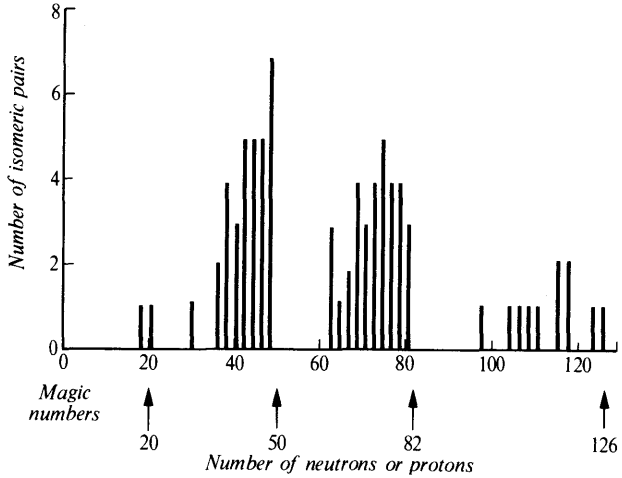

Fig. 9.6 Frequency distribution of odd-A isomeric nuclei (Ref. 2.1).

in terms of the single-particle shell model (Sect. 7.2.3) and form an important part of the evidence for the validity of this model.

An isomeric state is indicated by a superscript m, e.g. in Fig. 9.5 the states are $^{26}Al^{m}$, $^{77}Ge^{m}$ and $^{80}Br^{m}$.

9.3 Internal conversion

9.3.1 General

The lifetime formula of Weisskopf for radiative transitions gives the probability of decay of a bare point nucleus, completely stripped of the atomic electrons. Usually this is not the case, and since many electronic wavefunctions (in particular all wavefunctions of s-states) have finite amplitudes at or near the nucleus it is possible for nuclear excitation energy to be removed by the ejection of an atomic electron. The total probability per unit time of decay of the excited nucleus is then given by $\Gamma/\hbar$ where we write for a bound state

$$\Gamma = \Gamma_\gamma + \Gamma_e \tag{9.19}$$

in which Γ_e is the width for emission of electrons. In both cases the total energy of nuclear excitation is removed, but the electron emission process is generally described for historical reasons as internal conversion. This does not imply that the process follows the emission of radiation and the two processes must be regarded as competing alternatives. That this is so has been demonstrated by experiments in which the lifetime of a nucleus for isomeric decay

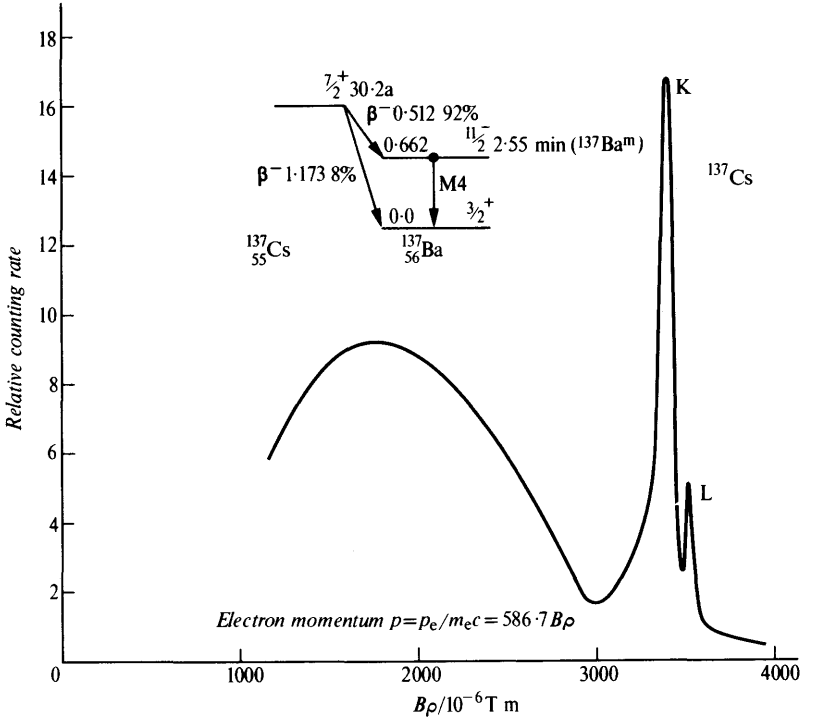

Fig. 9.7 Sketch of electron spectrum seen in a simple 180° spectrometer of the beta-decay electrons from ^{137}Cs, together with K and L internal conversion electrons from the 0.662 MeV transition in $^{137}Ba^m$. The decay scheme is shown, with energies in MeV. The K- and L-vacancies lead to X-ray emission from the Ba atom.

has been significantly altered by chemical control of its electronic environment.

Figure 9.7 shows the electron spectrum obtained in a magnetic spectrometer for the decay of ^{137}Cs, whose long life of 30a is due to the forbidden nature of its beta-particle emission. Superimposed upon the continuous distribution of electrons arising from the nuclear beta decay are sharp internal conversion lines resulting from the subsequent electromagnetic decay of the isomeric state $^{137}Ba^m$ with a halflife of 2·6 min. Gamma radiation corresponding with this transition is also observed and the energy E_γ of the transition may be obtained very accurately from the conversion spectra because the kinetic energy of an electron ejected from the K-shell is

$$E_\gamma - E_K \tag{9.20}$$

where E_K is the energy of the K-edge, which is known precisely

from X-ray data. In experimental observations the internal-conversion electrons must be distinguished carefully from photo-electrons produced externally by the gamma radiation. If the number of electrons observed per excited nucleus is N_e and the number of γ-rays is N_γ we define the *internal conversion coefficient* α as

$$\alpha = N_e/N_\gamma = \Gamma_e/\Gamma_\gamma \tag{9.21}$$

and α may have any value between 0 and ∞. From (9.19) it follows that if the total width Γ is determined then the radiative width Γ_γ is given by

$$\Gamma_\gamma = \Gamma/(1+\alpha) \tag{9.22}$$

or, in terms of mean lives,

$$\tau = \tau_\gamma/(1+\alpha) \tag{9.23}$$

High-resolution magnetic spectra show that for each γ-ray there are in fact several conversion lines corresponding to the ejection of electrons from different atomic shells, e.g. K, L_I, L_{II}, L_{III}, M_I, M_{II}, ... and the total conversion coefficient is, therefore

$$\left.\begin{aligned}\alpha &= (N_K + N_L + N_M + \cdots)/N_\gamma \\ &= \alpha_K + \alpha_L + \alpha_M + \cdots\end{aligned}\right\} \tag{9.24}$$

The difference in energy between the various groups of internal-conversion electrons corresponding with a single nuclear transition agree exactly with the energies of the lines of the X-ray spectrum of the atom containing the excited nucleus, e.g. Ba in the case shown in Fig. 9.7. The emission from an atom of an internal-conversion electron leaves a vacancy in one of the atomic shells. As in the case of the photoelectric effect with γ-radiation (Sect. 3.1.4), either K X-rays or Auger electrons or both may then be emitted.

The importance of the experimental study of internal conversion lies in the information that it may give about the multipolarity of the nuclear transition. The total conversion coefficient α is a ratio of intensities and if a nucleus of infinitesimal size is assumed it does not depend upon the nuclear matrix element. This matrix element arises naturally when the scalar Coulomb interaction between the atomic electron and the nucleus is expanded in multipoles; the conversion coefficients are found to be relatively higher for the higher multipoles. The interaction may be represented as due to an exchange of virtual photons and a factor α enters the conversion probability in this way, making it a second-order process overall.

Extensive tables of K- and L-conversion coefficients based on relativistic wavefunctions now exist. Figure 9.8 shows how the coefficient α_K varies with transition energy for a number of multipolarities in a typical nucleus. The rapid decrease of α with energy

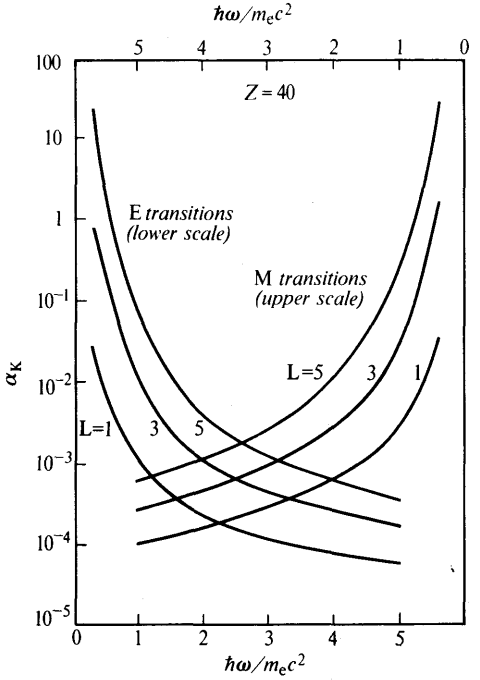

Fig. 9.8 Internal conversion coefficient α_K for $Z = 40$ (Blatt, J. B. and Weisskopf, V. F., *Theoretical Nuclear Physics*, Wiley, New York, 1952).

and the relatively poor discrimination between different multipolarities for high transition energies are made clear in this figure. Internal conversion coefficients are small for light atoms and their measurement is mainly useful for heavy elements and low transition energies.

Internal-conversion electrons from the L- and M-shells are also observable and the ratios of K to L and L to M intensities also depend on multipolarity. So do the relative intensities of internal conversion lines corresponding to the L- and M-subshells.

Corrections to internal conversion coefficients that are structure-dependent arise for a finite nucleus because the atomic electrons penetrate within the nuclear charge and current distribution. They are important for the E0 monopole transitions between states of zero spin (Sect. 9.3.3) for which internal conversion is the main mode of decay. These transitions may also compete with alternative transitions such as M1 or E2 when the spins of the initial and final states are the same and may become significant if the alternative transitions are retarded.

9.3.2 Pair internal conversion

If the transition energy E_γ exceeds $2m_ec^2$, i.e. if $E_\gamma > 1$ MeV, an excited nucleus may emit a positron–electron pair as an alternative to γ-ray emission and electron internal conversion. The theory of this process, which is electromagnetic in that it takes place in the Coulomb field of the excited nucleus, shows that the probability of pair internal conversion increases with transition energy, is greatest for small multipolarities and is almost independent of Z. These differences from ordinary internal conversion arise because the pair creation process according to hole theory requires only the elevation of an electron in a negative energy state to a positive energy and the supply of such electrons is unlimited, in contrast with the situation for ordinary electrons in an atom. Pair conversion thus becomes important under exactly the conditions under which ordinary internal conversion is becoming small and the phenomenon provides a powerful method of studying energetic radiative transitions in light nuclei. In such experiments care must be taken to distinguish between internal pairs and ordinary pair production in matter by the competing γ-ray.

Unfortunately, the theory of pair internal conversion shows that the discrimination between different multipoles is only good when the yield is low. A more sensitive method is to measure the angular correlation between directions of emission of the positron and the electron.

9.3.3 Zero–zero transitions

In the particular case of $I = 0$ to $I = 0$ transitions, single quantum radiation is strictly forbidden (Sect. 9.1) and the multipole fields do not exist outside the nucleus. The only contribution to internal conversion effects then involves electrons (such as the K-electrons) whose wavefunctions penetrate the nucleus, within which electromagnetic fields may still exist. Total internal conversion ($\alpha = \infty$) arising in this way is observed as a single homogeneous electron line, without associated γ-radiation, in the spectrum of RaC′ (1·414 MeV level) and of ^{72}Ge (0·7 MeV level). The lifetimes of these levels are longer than would be expected for radiative transitions of the particular energy and both transitions are assumed to be of the monopole or radial type $0^+ \rightarrow 0^+$. Pair internal conversion can also occur in $0^+ \rightarrow 0^+$ transitions and it is known for the first excited states of ^{16}O and ^{40}Ca.

Transitions of the form $0^+ \rightarrow 0^-$ cannot occur by any of the internal conversion processes just discussed. Two radiations are required, passing through a suitable virtual intermediate state, e.g. $0^+(\text{E1})1^-(\text{M1})0^-$ with the emission of two quanta would be a

possible mode of de-excitation. Alternatively, two conversion electrons or one conversion electron and one photon might be emitted.

9.4 Determination of transition probabilities

9.4.1 Mean lifetimes of bound states ($\tau_\gamma < 10^{-6}$ s)

(i) *Delayed coincidence method* ($\tau_\gamma \approx 10^{-6}$–$10^{-11}$ s). If the time of formation of a nuclear excited state by a nuclear reaction or decay process can be defined by an appropriate signal, and a further signal is obtained from the radiative decay itself, the probability of an interval t between the two signals is given by

$$P(t) = e^{-t/\tau_\gamma} \tag{9.25}$$

Experimentally it is convenient to delay the first signal by a time Δt and to find the time distribution of coincidences between the delayed signal and the decay pulse. This is given by

$$N_c(\Delta t) = N_0 e^{-\Delta t/\tau_\gamma} \tag{9.26}$$

and yields τ_γ directly.

This method can be applied to cascade radiative transitions in nuclear decay and to γ-radiation in a reaction such as X (p, p'γ)X in which the inelastically scattered proton provides the first signal. In the latter case, and for many similar nuclear reactions, the time delay in the particle emission is negligible in comparison with the lifetime under study and a pulsed accelerator beam may then be used to define the time of production of the excited state. Figure 9.9 shows the results of such an experiment on the reaction $^{16}O(d, p)^{17}O^*$ in which a special time-compression system was used to produce pulses of 10^{-10} s duration on the target.

Both Ge(Li) and scintillation detectors may be used in delayed coincidence circuits, the best timing being afforded by plastic scintillators. Wideband amplifiers are required in the timing circuits.

(ii) *Recoil distance method* (*RDM*) ($\tau_\gamma \approx 10^{-7}$–$10^{-12}$ s). If excited nuclei are produced in a nuclear reaction with sufficient (and known) velocity, the radiative lifetime may be found by studying the distribution of decay points along the path of a beam of such recoil particles. For $\beta = 0{\cdot}005$ and a decay time of 10^{-10} s the path length is 150 μm, a distance which may be determined by a mechanical assembly (micrometer head or *plunger*) or electrically by a capacitance measurement. The decay point is defined by a narrow collimator placed in front of the radiation detector.

The lifetimes of *atomic states* can be determined in a similar way using the technique of *beam foil spectroscopy*. Excited ions are produced by passing a beam of heavy ions through a thin foil and the intensity of radiation at right angles to the beam is determined as a function of distance from the foil.

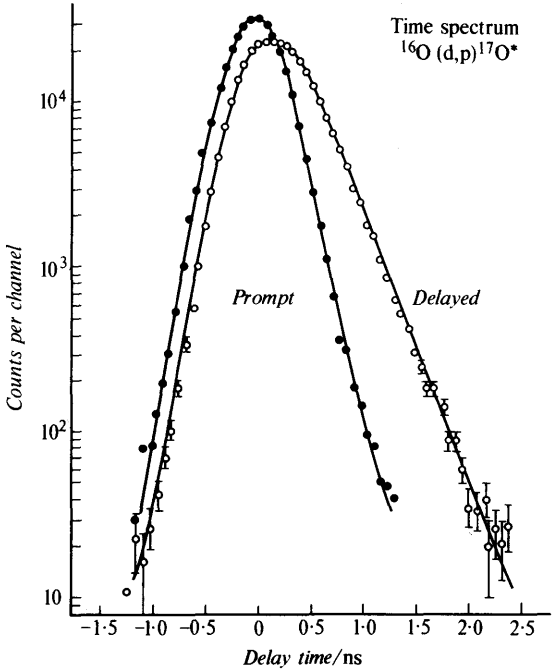

Fig. 9.9 Measurement of lifetime of 871 keV state of ^{17}O by delayed coincidence method, using a pulsed accelerator. The curve 'prompt' is for radiation from a state of effectively zero lifetime. A value $\tau_\gamma = (2{\cdot}63 \pm 0{\cdot}08) \times 10^{-10}$ s was obtained (Lowe, J. and McClelland, C. L., *Phys. Rev.*, **132,** 367, 1963).

The availability of Ge(Li) gamma-radiation detectors of high resolution has permitted an elegant development of the recoil distance method. If an excited nucleus emits a gamma ray while it is moving, the observed energy at angle θ with the direction of motion shows a Doppler shift and is $E_\gamma = E_0(1 \pm \beta \cos \theta)$; if the nucleus emits the radiation after it is brought to rest, the energy is unshifted, $E_\gamma = E_0$. If, therefore, the target is fixed and a stopping plate or plunger is used to receive the recoil ions, the spectrum observed at a certain angle with the beam direction and at a suitable distance shows two peaks whose relative height gives the fraction of nuclei decaying before and after reaching the plunger. This varies with plunger displacement and permits a direct calculation of lifetime; the recoil velocity is calculated from the reaction kinematics or obtained from the maximum observed Doppler shift, which can be an order of magnitude greater than the resolution width of the detector. Figure 9.10 shows results obtained by this method for the 871 keV state of ^{17}O formed in the reaction $^2H(^{16}O, p)^{17}O^*$. In all Doppler shift measurements it is advantageous to increase recoil

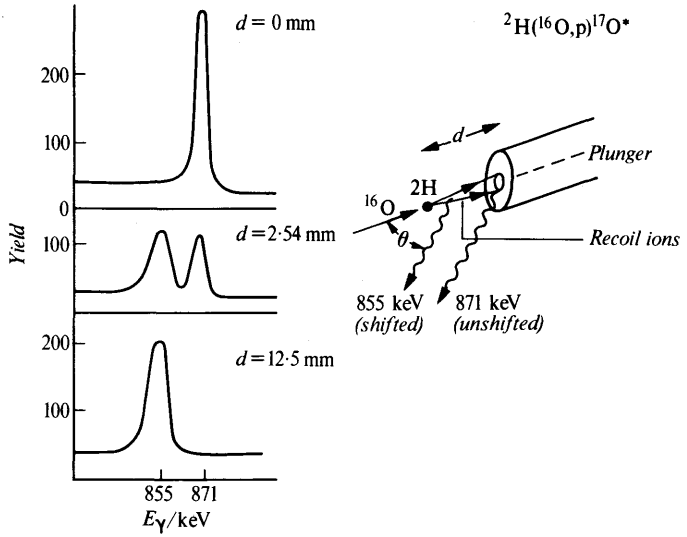

Fig. 9.10 Measurement of lifetime of 871 keV state of ^{17}O by RDM. Spectra are shown for three different plunger displacements and for an angle $\theta = 122°$. The lifetime deduced from the ratio of shifted to unshifted intensity was $(2{\cdot}33 \pm 0{\cdot}26) \times 10^{-10}$ s (adapted from Allen, K. W., *Electromagnetic Interaction in Nuclear Spectroscopy*, Ch. 9, North Holland, 1975).

velocities by the use of heavy rather than light projectiles whenever possible; in the case of ^{17}O, a deuterium target and ^{16}O beam were used.

(iii) *Doppler shift attenuation method* (*DSAM*) ($\tau_\gamma \approx 10^{-11}$–$10^{-14}$ s). For lifetimes less than 10^{-11}–10^{-12} s the recoil distance method becomes difficult because plunger displacements of $< 10^{-5}$ m have to be measured accurately. It is, however, still possible to use the Doppler shift to measure these lifetimes. The principle of the method is to relate the energy *spectrum* of the radiation from a beam of recoiling nuclei to the ratio between the radiative lifetime τ_γ of the excited state and the time (α) that the recoil nuclei take to slow down in an absorber. If $\tau_\gamma/\alpha \ll 1$ then nearly all decays will show the full Doppler shift $\Delta E_{\gamma 0} = E_0 \beta \cos\theta$, while if $\tau_\gamma/\alpha \gg 1$ most of the decays are unshifted. If an attenuation factor $F(\tau_\gamma)$ is defined to be the percentage of the full Doppler shift $E_{\gamma 0}$ observed in a given spectrum then in these two extreme cases $F = 1$ and 0 respectively and only upper and lower limits can be established. In intermediate cases $0 < F(\tau_\gamma) < 1$, a value for τ_γ can be obtained.

In practical applications of the DSAM the recoil direction is often defined to a few degrees by requiring observations to be coincident with the detection of an associated reaction particle (usually at 180° with the beam direction to give maximum recoil velocity). The

excited nuclei recoil into the target backing and slow down to rest. Their radiation, Doppler shifted according to their velocity, is detected over a certain range of angles by a Ge(Li) detector located at a known mean angle with the recoil direction.

The simplest analysis is to determine the centroid of the shifted line over a range of angles. From the indicated $F(\tau_\gamma)$ the lifetime τ_γ may be inferred. If good resolution is available and the Doppler shift is large enough, more information may be obtained from a detailed analysis of the line shape using τ_γ as a parameter. In both cases electronic and nuclear stopping-power data must be used and account taken of the scattering of recoils by nuclear collisions; the full Doppler shift $\Delta E_{\gamma 0}$ may be obtained by direct observation or by calculation using reaction kinematics.

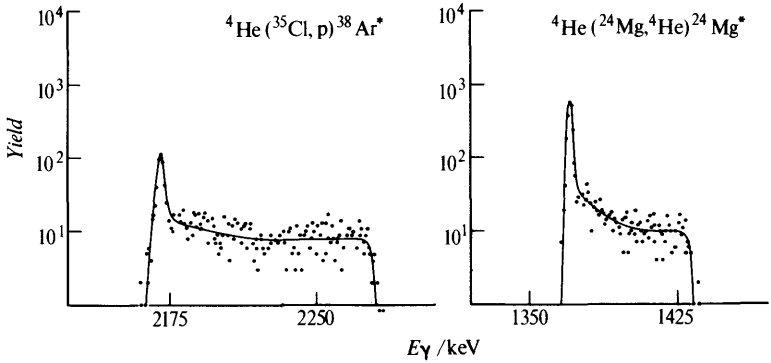

Fig. 9.11 Measurement of lifetime of 2168 keV state in ^{38}Ar and of 1368 keV state in ^{24}Mg by DSAM, line-shape analysis. Lifetimes of 0·72 and $1{\cdot}82\times10^{-12}$ s (±7%) were deduced (adapted from Forster, J. S. *et al.*, *Phys. Letters*, **51B**, 133, 1974).

Figure 9.11 shows results obtained for ^{38}Ar* and ^{24}Mg* by heavy-ion bombardment of a ^{4}He target leading to lifetimes of about 10^{-12} s. The accuracy of DSAM results may be impaired by systematic errors due to lack of knowledge of stopping powers for slow heavy ions in matter. These errors are reduced if high recoil velocities can be used and an accuracy of about 5 per cent is attainable.

9.4.2 Coulomb excitation

The radiative lifetime measurements described in the preceding sections cover the region from the 'isomeric' lives of 10^{-6} s down to about 10^{-15} s, which corresponds with a width of 0·6 eV. It is, however, not always convenient to produce the recoil velocities necessary for measurement of the shorter lives. Fortunately,

phenomena that are determined by the radiative *width* become easier to observe as the mean life diminishes and may be used to measure transition probabilities when direct lifetime measurements are impracticable. A generally applicable method is that of Coulomb excitation.

A charged particle passing near to a nucleus with an energy considerably less than the height of the mutual potential barrier so that nuclear effects may be disregarded, follows a classical trajectory prescribed by the Coulomb force $Z_1Z_2e^2/4\pi\varepsilon_0 r^2$ acting between mass centres. The total interaction however, for a finite target nucleus, must recognize the effect of the charge and current distributions. This may be described by making a multipole expansion of the scalar interaction and this in turn introduces the multipole matrix elements and reduced transition probabilities $B(L)\uparrow$ that apply in photon absorption (e.g. in the transition $f \rightarrow i$ in Fig. 9.2). The process is detected by observation of the de-excitation radiation ($i \rightarrow f$ in Fig. 9.2).

The cross-section for Coulomb excitation depends on the particle trajectory, which may be calculated, as well as on $B(L)$. The effect of multipolarity on transition probability indicated in Section 9.1.3 is less severe for Coulomb excitation than for spontaneous emission, because the effect is extra-nuclear. There is, however, an inhibition of magnetic transitions with respect to electric transitions of the same multipolarity by a factor $\approx(v/c)^2$ where v is the projectile velocity. Yield curves, such as that shown for ^{181}Ta in Fig. 9.12, may be used to determine the probability and multipolarity of a transition.

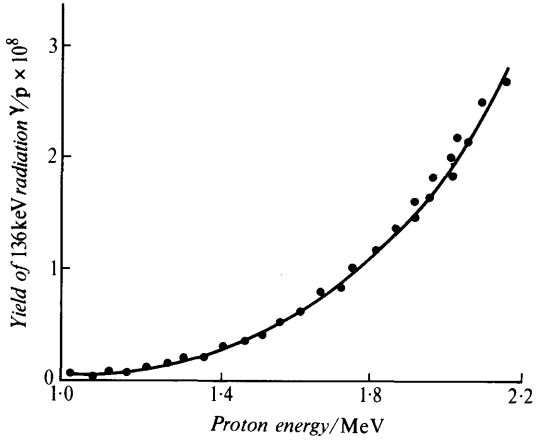

Fig. 9.12 Yield of 136-keV quanta from ^{181}Ta bombarded by protons as a function of proton energy, compared with theory for E2 excitation (solid curve) (Huus, T. and Zupančič, C., *Det. Kgl. Dansk. Vid. Selskab.*, **28,** 1, 1953).

Coulomb excitation has been observed throughout the periodic system and with many types of bombarding particle, including heavy ions such as ^{14}N and ^{40}A, which are particularly effective because of their high charge. An important application is in the study of rotational levels excited by E2 transitions and in fact a great many Coulomb excitation processes are of E2 type. In cases when $|\Delta I| = 1$ the subsequent radiative transition may be a mixture of M1 and E2 components and analysis of the mixture may be made by the methods normally applied to radioactive decay schemes.

The use of heavy ions has permitted the observation of higher-order processes, e.g. the excitation of a 4^+ level in an even–even nucleus by the double E2 sequence $0^+ \rightarrow 2^+ \rightarrow 4^+$. Another double E2 process of some importance is the *reorientation* effect in which a state of spin I which has been Coulomb-excited makes an E2 transition from one magnetic substate (I, m') to a second substate (I, m'') as a result of interaction of the electric field of the bombarding particle with the electric quadrupole moment Q of the exicted state. The effect is a useful method for determination of this moment.

9.4.3 Inelastic scattering of electrons

Coulomb excitation by electrons is in principle possible, but in practice it is difficult to observe as an emission process because of the presence of bremsstrahlung quanta. The inelastically scattered electrons, however, may be observed with good discrimination against background at large angles of scattering, and the spectrum then shows peaks corresponding with the excitation of the lower excited levels of the target nucleus, in addition to the ground-state (elastic) peak. As with heavy-particle Coulomb excitation, the interaction between an electron and the nucleus may be expanded in multipoles, but no restriction on particle velocity is necessary in order to avoid nuclear effects. Magnetic transitions may, therefore, be more easily observed. Moreover, in ordinary Coulomb excitation only the normal (transverse) radiative matrix elements occur but in electron excitations the (longitudinal) static Coulomb interaction also contributes. This contains a monopole component so that $0^+ \rightarrow 0^+$ transitions may be excited. The most important difference between the two techniques, however, is the fact that in inelastic scattering the momentum transfer $\boldsymbol{q}$ to the nucleus may be varied independently of energy transfer, and the momentum dependence of matrix elements may be explored.

As in the case of elastic scattering (eqn (6.7)) the observed cross-section as a ratio to that for Mott scattering may be described by the quantity $|F(q)|^2$ where $F(q)$ is a form factor determined by matrix elements of the multipole operators. From the variation of

scattering cross-section with q the ground-state charge density may be obtained for elastic scattering, and a 'transition' charge density in the inelastic case. This can be compared with the prediction of nuclear models.

In general, there are three form factors to be considered in an electron inelastic scattering experiment, namely $F_C(q)$, $F_e(q)$ and $F_m(q)$ corresponding with the longitudinal (or Coulomb) and transverse excitations, magnetic excitations being wholly transverse. The longitudinal form factor may be separated experimentally by observations at different angles for a given q. For low-momentum transfers the Coulomb transition probability reduces essentially to the electric multipole probability for the same L-value. Extrapolation of $F_C^2(q)$ to the 'photon' point corresponding to the actual transition energy, which is essentially $q \rightarrow 0$, then determines the upward transition probability $B(L)\uparrow$ to the excited state, while the spin-parity of the state and its transition charge density follow from the q-dependence of F_C^2.

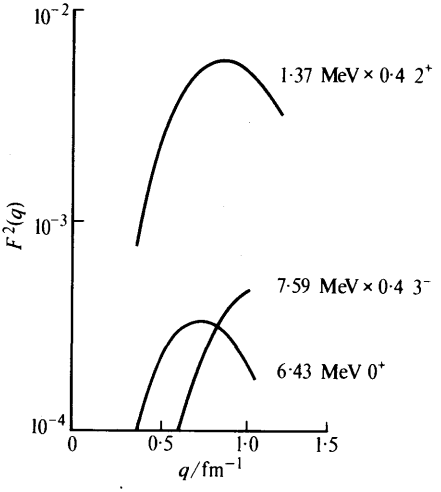

Fig. 9.13 Inelastic form factor for the scattering ^{24}Mg(e, e')^{24}Mg*, showing variation with momentum transfer q for a 0^+, 2^+ and 3^- transition (derived from Johnston, A. and Drake, T. E., *J. Phys.*, **A7**, 898, 1974).

Figure 9.13 shows this dependence for three transitions in ^{24}Mg, using electron energies of about 100 MeV and scattering angles of about 120°; one of the transitions is a monopole. For the 1·37 MeV level the $B(L)\uparrow$ value leads to a lifetime of $2{\cdot}0 \pm 0{\cdot}2$ ps in agreement with other methods (Sect. 9.4.1).

In inelastic electron scattering the kinematic factor $(kR)^2$ that reduces the intensity of high multipoles in spontaneous emission

(eqn (9.8)) is replaced by $(qR)^2$ where q is normally very much greater than k (e.g. $q \approx 1\,\text{fm}^{-1}$, $k \approx 10^{-3}\,\text{fm}^{-1}$). It follows that high-spin states can often be excited.

9.4.4 Nuclear resonance reactions

Suppose that the level i shown in Fig. 9.2 exists in a nucleus C, which may be represented as C* when excited. It may then be possible to produce the excitation by capture of a bombarding particle (a) in a suitable initial nucleus X, i.e.

$$\text{X} + \text{a} \rightarrow \text{C}^* \tag{9.27}$$

These processes are of great importance for the theory of nuclear reactions and were discussed in Section 8.1. For the present purpose we note only that the cross-section for the emission of radiation from C* by the process

$$\text{C}^* \rightarrow \text{C} + \gamma \tag{9.28}$$

assuming just one possible transition of energy $E_\gamma = E_i - E_f$ to the ground state f is

$$\sigma_{a\gamma} = \pi \lambda\!\!\!^{-2} g \Gamma_a \Gamma_\gamma / [(T - T_0)^2 + \Gamma^2/4] \tag{9.29}$$

where $\lambda\!\!\!^{-}$ is the c.m. wavelength of the bombarding particle a, T is the c.m. energy, T_0 is the c.m. energy at which there is exact resonance with the level E_i, and g is a statistical factor of the order unity depending on intrinsic spins. This is an example of the Breit–Wigner formula (Sect. 11.2) which has the present simple form when only one l-value contributes to the reaction; the value of g is given by equation (11.16).

In the present case the level i is virtual and is at an energy above the ground state f equal to T_0 plus the separation energy of particle a in nucleus C (cf. Fig. 11.6). The width Γ of the level measures the total probability of decay and in this case includes the width Γ_a for re-emission of the incident particle, together with the radiative width Γ_γ and the internal conversion width $\alpha\Gamma_\gamma$. If there are no other decay modes then

$$\Gamma = \Gamma_a + \Gamma_\gamma(1 + \alpha) \tag{9.30}$$

The internal conversion coefficient (Fig. 9.8) is normally negligible for $E_\gamma > 1\,\text{MeV}$ and need not be included for high-energy capture transitions, $E_\gamma \approx 8$–$12\,\text{MeV}$.

At resonance, $T = T_0$, the absorption cross-section is

$$\sigma_a = 4\pi \lambda\!\!\!^{-2} g \Gamma_a \Gamma / \Gamma^2 = 4\pi \lambda\!\!\!^{-2} g \Gamma_a / \Gamma \tag{9.31}$$

whereas the cross-section for production of radiation is

$$\sigma_{a\gamma} = 4\pi \lambda\!\!\!^{-2} g \Gamma_a \Gamma_\gamma / \Gamma^2 \tag{9.32}$$

If $\Gamma_a \gg \Gamma_\gamma$, the scattering cross-section yields $g\Gamma_\gamma/\Gamma$ and if Γ is known from the variation of yield with energy then $g\Gamma_\gamma$ for the level i can be obtained. This case arises for *proton and α-particle capture* in light elements at energies somewhat below the barrier height, for which $\Gamma_a \approx 10$ keV and $\Gamma_\gamma \approx 1$ eV.

If $\Gamma_a \ll \Gamma_\gamma$, then the resonant cross-section $\sigma_{a\gamma}$ yields $g\Gamma_a/\Gamma$ and $\Gamma_\gamma (\approx \Gamma)$ may be obtained from the variation of yield with energy. This case arises for *slow-neutron capture*, when $\Gamma \approx 0{\cdot}1$ eV, $\Gamma_n \approx 10^{-3}$ eV and the virtual levels concerned are within a few electron volts of the neutron binding energy.

A special case of a resonance reaction arises when a is a photon and the only process possible is photon scattering. The Breit–Wigner formula is not strictly applicable in this case and should be replaced by the *Lorentzian* expression for the scattering of radiation by an oscillator. The difference, however, is not usually significant at energies near resonance and the Breit–Wigner form will be used. It is now possible for the level i to be bound, and of low excitation, so that it is necessary to take account of internal conversion. The absorption cross-section for monochromatic radiation at resonance then becomes

$$\sigma_\gamma = 4\pi\lambda^2 g/(1+\alpha) \tag{9.33}$$

and for radiation of energy 500 keV this is of the order of 10^4 b.

The total electronic cross-section for attenuation of radiation of an energy of 500 keV in a light element such as oxygen or carbon is of the order of 10^2 b. It might therefore be expected that nuclear attenuation could be easily observed by increasing the energy of the incident radiation until resonance absorption appeared. However, if a bremsstrahlung spectrum is used for the experiment it is necessary to average the nuclear cross-section over the energy interval ΔE accepted at one setting of the detector. When equation (9.29) is averaged in this way (essentially by integration between energies plus and minus infinity) the mean absorption cross-section becomes

$$\bar{\sigma}_\gamma = 2\pi^2\lambda^2 g\Gamma_\gamma/\Delta E \tag{9.34}$$

and since the factor $\Gamma_\gamma/\Delta E$ may be 10^{-4} or less, the nuclear effect becomes small compared with electronic absorption. Discrimination against the latter is achieved by observing scattered intensities at backward angles, since the non-resonant electronic scattering is peaked in the forward direction. In this way radiative widths Γ_γ of levels of width $\approx 0{\cdot}5$ eV have been observed for a number of light elements.

For the narrowest states, say $\ll 0{\cdot}5$ eV, it is usually necessary to use resonance radiation, as in optics, to excite a level by means of the radiation emitted in the decay of the same level in an active source or target. The absorption cross-section at exact resonance

given by (9.33) does not determine Γ_γ, since this quantity has cancelled out, but in practice this particular situation is drastically altered in a useful way by the existence of Doppler shifts and recoil effects.

In the emission of the resonance radiation of energy E_γ from a stationary source atom of mass M, a momentum $p = E_\gamma/c$ must be imparted to the emitting body. In the absorption process the same momentum must be given to the absorber atom. The emission and absorption lines are therefore separated, because of recoil, by an energy

$$2 \times p^2/2M = E_\gamma^2/Mc^2 \tag{9.35}$$

In addition, both source and absorber atoms are normally affected by thermal motion and the lines are broadened by the Doppler effect in liquids and gases and by the width of associated phonon transitions in solids. The recoil effect is negligible in atomic transitions and resonance absorption of broadened lines takes place, as shown in Fig. 9.14*a*. For a *nuclear* transition with free recoil, on the other hand, the recoil shift is always $\gg \Gamma_\gamma$ for low-lying bound levels, and is often greater than the Doppler width. Nuclear resonance is, therefore, a weak effect unless recoil losses are restored or eliminated; the situation is as shown in Fig. 9.14*b*. The introduction of the recoil and thermal terms into (9.33) creates a dependence of the resonant cross-sections on Γ_γ itself and permits measurement of this quantity if a sufficient effect can be achieved.

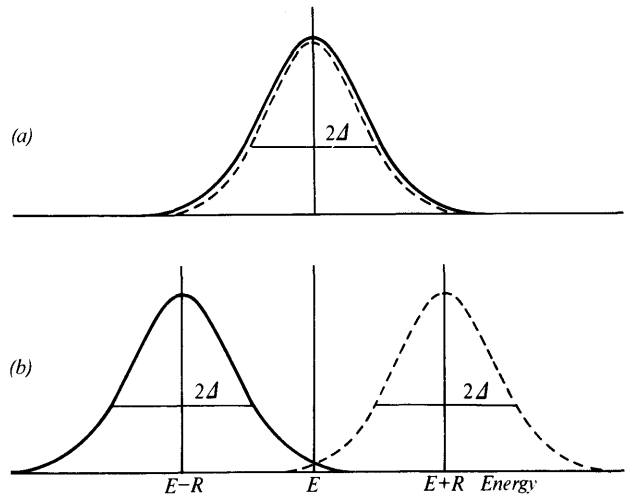

Fig. 9.14 Effect of recoil on atomic and nuclear resonance. The solid line represents the intensity distribution of the incident radiation and the dotted line the absorption cross-section of the absorber as a function of (homogeneous) incident energy. (*a*) Atomic resonance, recoil shift $R \ll$ Doppler width Δ. (*b*) Nuclear resonance, $R > \Delta$.

Recoil energy loss can be restored, and resonance between Doppler-broadened lines obtained, by the following means:

(*a*) By mounting a radioactive source on the tip of a high-speed rotor and using the Doppler effect to increase the frequency of the emitted radiation. From (9.35) the speed required is given by

$$E_\gamma(v/c) = E_\gamma^2/Mc^2 \tag{9.36}$$

and for a nucleus of mass 200 and $E_\gamma = 500\,\text{keV}$ the value $v = 820\,\text{m s}^{-1}$ is found.

(*b*) By heating the radioactive source so that the Doppler or phonon broadening is largely increased. Temperatures of up to 1500 K have been used.

(*c*) By utilizing a preceding transition, such as β-decay, γ-decay or production in a nuclear reaction to provide the necessary velocity for Doppler shift of frequency.

Like Coulomb excitation, nuclear resonance shows largest effects in cases of large width, i.e. of small lifetime. The method is rather more limited than Coulomb excitation since gram quantities of the scatterer are required and it may be difficult to supply the velocity necessary to restore the recoil effect. Despite this, radiative widths have been obtained for many transitions by the resonance method and cover a range of lifetimes from 10^{-9} to 10^{-13} s.

Recoil energy loss in a gamma-ray resonant scattering or absorption experiment can be eliminated without associated broadening due to phonon transitions, in certain special cases. It was discovered by Mössbauer in 1958 that the radiation from a source of ^{191}Ir contained a narrow line of approximately natural width Γ_γ ($\approx 10^{-5}$ eV) as well as the expected thermal distribution. Nuclear resonance in an iridium absorber could be destroyed by motion of the source, with a velocity of less than 40 mm s^{-1}. Such narrow lines correspond to processes in which *no* phonon transitions take place, and they are unshifted because for photon energies less than about 200 keV the recoil energy is insufficient to remove the atom from its lattice site and the effective mass in equation (9.35) is that of the crystal as a whole, which absorbs momentum, but not energy, in the transition. Similar considerations were shown by Lamb, as early as 1939, to apply to the scattering of slow neutrons by crystals.

Although Mössbauer transitions have been observed in many nuclei, the limitation to low transition energies is rather restrictive. Moreover, the pure natural line width may not be observed, because of broadening by hyperfine interactions in the source and absorber. As far as nuclear physics is concerned, the effect has mainly exploited the high resolution available ($\Gamma_\gamma/E_\gamma \approx 10^{-13}$) and has been

used, sometimes in conjunction with other techniques such as nuclear magnetic resonance (NMR), to measure nuclear magnetic moments and quadrupole moments of excited states and the isomer shifts which arise from the difference between the mean-square radius of nuclear ground and excited states. The applications of the Mössbauer effect in solid state physics, metallurgy and chemistry are extensive (Ref. 9.2).

9.5 Angular correlation experiments

9.5.1 Angular distribution of radiation

The most direct indication of the multipolarity L of a radiative transition is the angular distribution of the intensity of the radiation corresponding to a transition between initial and final substates $(I_2 m_2)$ and $(I_1 m_1)$ of two levels (Fig. 9.15). The axis of quantization is fixed experimentally, e.g. by the direction of an external magnetic field.

For atomic transitions it is well known from the Zeeman effect that the magnetic substates may easily be separated magnetically and the individual components of a line, two of which are shown in Fig. 9.15, may be studied. In the nuclear case, because of the

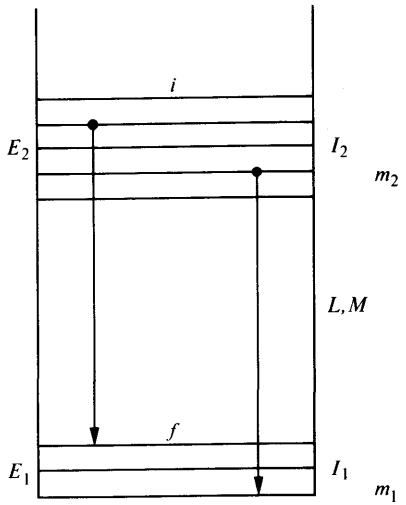

Fig. 9.15 Radiative line of multipolarity L between two nuclear levels of spin I_2 and I_1, each of which has $2I+1$ substates characterized by the magnetic quantum number m. Two of the possible transitions (L, M) are indicated. If no perturbing fields act on the radiating nucleus the substates for a given I all have the same energy although they are shown distinct.

smallness of nuclear moments, a separation comparable with the experimental resolution is only possible under special conditions, such as those offered by the Mössbauer effect (Sect. 9.4.4). The total line, rather than its individual incoherent components, is then observed from an assembly of excited nuclei.

If in such an assembly the substates m of the initial level are uniformly populated the angular distribution of the line intensity is isotropic. If, however, the substate population $P(m)$ depends on m, the assembly is said to be *spin-oriented.* The case $P(m) = P(-m)$ defines an *aligned* system whereas if $P(m) \neq P(-m)$ the system is said to be *polarized.* The line intensity for an oriented system will, in general, be anisotropic.

The probability of the vectors $\boldsymbol{I}_1$, $\boldsymbol{L}$ combining to give a vector $\boldsymbol{I}_2$ with particular magnetic quantum numbers, is given by the Clebsch–Gordan coefficients, discussed in Appendix 4. The angular distribution arising from a given substate m_2 of the initial level can then be written

$$W(\theta) = \sum_{m_1} (I_1 L m_1 M \mid I_2 m_2)^2 F_L^M(\theta) \tag{9.37}$$

where $F_L^M(\theta)$ is the angular distribution for the appropriate multipole field (Sect. 9.1), and is in fact the modulus squared of a vector spherical harmonic (Sect. 9.1.2). The quantum numbers L, M for the emitted radiation are limited by the selection rules (9.3), i.e.

$$I_2 + I_1 \geqslant L \geqslant |I_2 - I_1|$$
$$m_2 = M + m_1$$

If the initial substates have a weight $P(m_2)$ the total angular distribution is

$$W(\theta) = \sum_{m_1 m_2} P(m_2)(I_1 L m_1 M \mid I_2 m_2)^2 F_L^M(\theta) \tag{9.38}$$

This must reduce to a constant if $P(m_2)$ is independent of m_2, in which case the initial levels are equally populated (random orientation). Thus, for example, if $I_2 = 1$, $I_1 = 0$, $L = 1$ (dipole) radiation is emitted; the specific angular distributions are $F_1^0 \propto \sin^2\theta$, $F_1^{\pm 1} \propto (1 + \cos^2\theta)/2$ and the Clebsch–Gordan coefficients are

$$(010 \pm 1 \mid 1 \pm 1) = 1, \qquad (0100 \mid 10) = 1$$

so that

$$W(\theta) \propto \sin^2\theta + 2 \times \tfrac{1}{2}(1 + \cos^2\theta)$$

= constant, as expected.

The functions $F_L^M(\theta)$ contain only Legendre polynomials of even order for pure multipole radiation so that we may also write

$$W(\theta) = a_0 + a_2 \cos^2\theta + a_4 \cos^4\theta + \cdots + a_{2L} \cos^{2L}\theta \quad (9.39)$$

which expresses the result that no term in $\cos\theta$ of power higher than $2L$ appears. The distribution is symmetric with respect to the plane $z = 0$, a consequence of the conservation of parity, i.e. invariance under the inversion operation, for the electromagnetic interaction.

The observation of a multipole angular distribution does not determine the electric or magnetic character of the transition, i.e. the parity change, since E1 and M1 radiation, for instance, have the same angular distribution patterns. A distinction may be made if the polarization of the radiation, e.g. the direction of the electric vector, can be observed.

Generally, the selection rules for radiation allow more than one multipolarity in the transitions $I_2 \rightarrow I_1$. The corresponding angular distribution with respect to the quantization axis then involves the mixing ratio δ, which is a model-dependent quantity of considerable interest.

9.5.2 Experimental methods

Nuclei may be oriented with respect to an axis of quantization defined by an external field by the application of a high magnetic field B_0 at low temperatures. If the normal Boltzmann distribution of nuclei between the magnetic substates is to be appreciably disturbed it is necessary to use fields and temperatures related by

$$\mu_I B_0 \approx kT \quad (9.40)$$

where μ_I is the nuclear magnetic moment. For $\mu_I = 1$ nuclear magneton this gives $B_0/T = 2{\cdot}8 \times 10^3$ tesla K^{-1}. Radioactive nuclei such as ^{60}Co, leading to daughter nuclei in which radiative transitions take place, have indeed been studied by this method.

The extreme conditions required by the direct orientation method soon led to the development of methods in which internal atomic fields, guided by a much smaller external field, produce the orientation. Dynamical methods in which the Boltzmann distribution is disturbed by microwave transitions or optical pumping techniques are also used, especially for the production of polarized beams and targets for accelerator experiments. For the study of radiative transitions, however, the most widely used technique has been that of angular correlation of successive radiations.

Figure 9.16*a* shows states of spin I_2, I_1, I_0 of a nucleus, linked by pure multipole transitions L_a, L_b. The first decay $I_2 \rightarrow I_1$ produces a non-uniform population of the substates of state I_1, with respect to

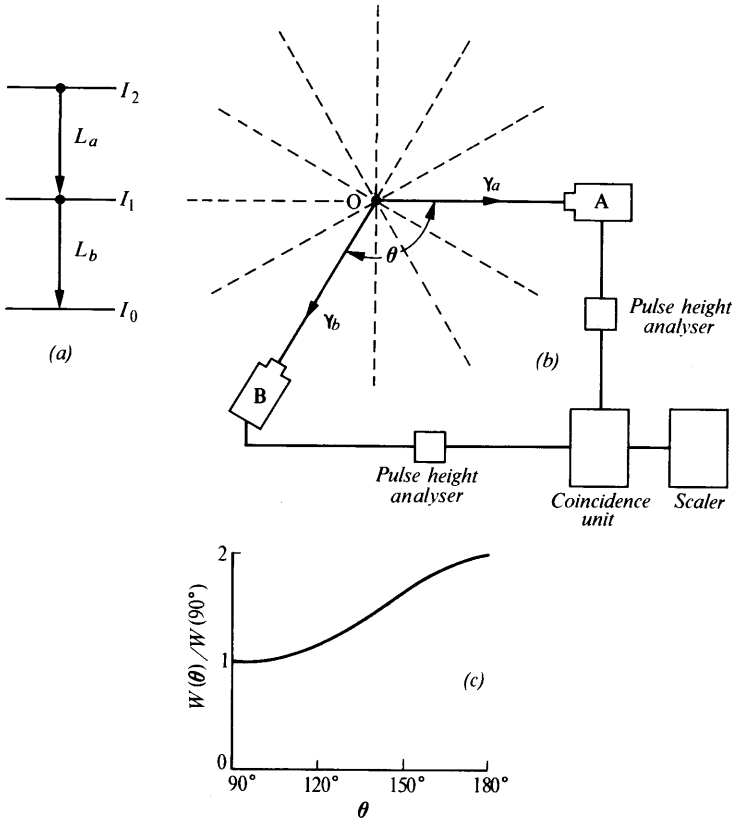

Fig. 9.16 Angular correlation of successive radiations from a radioactive nucleus at O. (*a*) Decay scheme. (*b*) Counters. (*c*) Correlation pattern.

an axis of quantization defined by the direction of emission of the photon γ_a (Fig. 9.16*b*). The nucleus I_1 is *aligned* with respect to this axis, since the first transition produces no difference between the substates of I_1 with equal and opposite m-values. The relative population is given explicitly by the expression

$$P(m_1) = \sum_{m_2} (I_1 L_a m_1 M_a \mid I_2 m_2)^2 F^{M_a}_{L_a}(0) \tag{9.41}$$

where

$$m_2 = M_a + m_1 \tag{9.42}$$

and the choice of axis restricts M_a to the values ∓ 1 corresponding to left or right circular polarization of the photon γ_a observed at $\theta = 0°$. The directional correlation γ_a, γ_b (Fig. 9.16*c*) is then given

by

$$W(\theta) = \sum_{m_0 m_1 m_2} (I_1 L_a m_1 \pm 1 \mid I_2 m_2)^2 F^{\pm 1}_{L_a}(0) \times (I_0 L_b m_0 M_b \mid I_1 m_1)^2 F^{M_b}_{L_b}(\theta) \quad (9.43)$$

where

$$m_1 = M_b + m_0 \quad (9.44)$$

assuming that the state decays before its alignment is disturbed by perturbing fields.

In the particular case $I_2 = I_0 = 0$, $I_1 = 1$ the transitions permitted when γ_a is observed at 0° are $(I, m) = (0, 0) \rightleftarrows (1, \pm 1)$. If the appropriate Clebsch–Gordan coefficients are inserted in (9.43) the angular correlation is given by

$$W(\theta) \propto F^{\pm 1}_1(0)[F^1_1(\theta) + F^{-1}_1(\theta)]$$
$$\propto 1 + \cos^2 \theta$$

Similar calculations may be made for more complicated cascades but the numerical evaluation of the correlation function becomes very tedious because of the large number of summations over magnetic quantum numbers which are necessary. Fortunately, it is possible to avoid this through algebraic methods developed by Racah and it is now customary to write the general angular correlation function for transitions of pure multipolarity in the form

$$W(\theta) = \sum A_\nu P_\nu(\cos \theta) \quad (9.45)$$

where

$$\nu = 0, 2, 4, \ldots$$

and

$$A_\nu = F_\nu(L_a I_2 I_1) F_\nu(L_b I_1 I_0) \quad (9.46)$$

The functions F_ν are tabulated in Reference 9.3.

A typical experimental arrangement for the observation of angular correlations in cascade transitions is shown in Fig. 9.16*b*. The detector pulses are combined in the coincidence unit and the number of coincidences $W(\theta)$ is determined as a function of the angle between the counter axes. The anisotropy

$$\varepsilon = \frac{W(\frac{1}{2}\pi) - W(0)}{W(\frac{1}{2}\pi)} = \frac{W(90°) - W(180°)}{W(90°)}$$

can be compared with that predicted by (9.43) or a complete curve for $W(\theta)$ (Fig. 9.16*c*) may be obtained.

The formulae can be extended to include multipole mixing, and to permit evaluation of the mixing ratios for the pure multipoles

permitted by the spin change. Polarization-sensitive detectors enable the parity change to be found.

9.6 Comparison between experiment and theory

In order to compare the matrix elements of multipole operators with the predictions of nuclear models, it is first of all necessary to establish the multipolarity of a transition, or the contributing multipolarities if it is mixed. Usually, one particular experiment does not provide the required information, but a combination of angular correlation data with internal conversion measurements may do so. At the same time the electric or magnetic multipole character of the radiation must be obtained, often from the energy–lifetime relations themselves, but sometimes from polarization measurements. When the appropriate L^{π} is known it is possible to extract the reduced transition probability $B(L)$ for a pure multipole from measurements of $T(L)$.

For a given multipole, the *transition strength* $|M|^2$ is conventionally measured in Weisskopf units (w.u.) using equation (9.15), i.e.

$$|M|^2 = \frac{T(L)\text{ observed}}{T(L)\text{ Weisskopf}} = \frac{B(L)\text{ observed}}{B(L)\text{ s.p.}} \tag{9.47}$$

where $B(L)$ s.p. indicates that the single-particle model is being used. This reduction of data has been extensively used for nuclei of mass number up to 40 though it is not confined to this range. For heavy deformed nuclei comparison may alternatively be made with the Nilsson model.

In terms of $|M|^2$, the following conclusions emerge:

(*a*) E1 transitions in the light nuclei have $|M|^2 \approx 0.03$. If the transition is isospin forbidden, as in the case of $\Delta T = 0$ transitions in self-conjugate nuclei, $|M|^2 \approx 0{\cdot}003$. The transition strength is then due to isospin admixtures in the nuclear states as a result of Coulomb forces, and the matrix element of the Coulomb interaction between the two states may be obtained from the observed strength.

(*b*) M1 transitions in the light nuclei, if isospin-favoured, have about the Weisskopf strength. For $\Delta T = 0$ transitions in self-conjugate ($N = Z$) nuclei there is retardation by a factor of about 10 because of some cancellation between the neutron and proton magnetic moments.

(*c*) E1 and M1 transition strengths in medium-weight and heavy nuclei have been surveyed by the (n, γ) capture reaction and are generally less than 1.

(*d*) E2 strengths in both light and heavy nuclei also show a dependence on isospin, but in this case are retarded in self-conjugate

nuclei for $\Delta T = \pm 1$. The T-allowed transitions may have strengths up to 100 for deformed nuclei.

(*e*) E3 and M4 transitions from isomeric states show relatively little spread of transition strength.

(*f*) There is no apparent difference in strength between transitions associated with a single odd neutron or a single odd proton.

The interpretation of the observed strengths follows the procedures already outlined for static moments (Ch. 8). For all but pure single-particle levels, the single-particle strength must be distributed among all transitions between states that derive from the basic levels, so that any specific transition has a reduced strength.

Calculations have been based on the individual-particle model for light nuclei near closed shells. As the number of loose particles increases, this type of calculation becomes difficult in detail, but still suggests that the single-particle transition probability should be multiplied by a factor (<1) depending on the number of available particles. Further away from closed shells the individual particle merges into the collective model as has already been discussed, and an explanation of the large observed E2 strengths is provided in terms of coherent motion of nucleons.

9.7 Summary

The electromagnetic interaction is well-described by Maxwell's equations and a complete classical theory exists. The electromagnetic field may be quantized by the introduction of the massless photon and many electromagnetic processes may be described in terms of single photon exchange. No breakdown of the laws of the interaction has been found even for interparticle distances of the order of 10^{-15} m; the electron and the muon behave essentially as point charges. These particles are therefore highly suitable for exploring nuclear charge distributions and this application is described.

Because the interaction is known, a precise formulation of the electromagnetic matrix element for a transition between two states may be given. Its properties determine selection rules for the transition and its squared magnitude gives the transition probability. Methods of measuring multipolarities and transition probabilities are reviewed and the information thus obtainable on the wavefunctions of the states involved is outlined.

Examples 9

9.1 Write down possible intrinsic and orbital angular momenta for the following radiations:

electric dipole (E1) electric quadrupole (E2)

magnetic dipole (M1) magnetic quadrupole (M2)

given that the parity of the multipole field EL is $(-1)^L$ and of ML is $-(-1)^L$. Assume that L^π for the photon is 1^-.

9.2* In the ^{207}Pb nucleus the magnetic moment of the ground state is 0·59 nuclear magnetons and the halflife of the first excited state at 570 keV is 130 ps. Use this information, together with equations (7.10), (7.11) and (9.18), to deduce the single-particle character of the two states.

9.3* In the decay of $^{137}_{55}$Cs (Fig. 9.7) the 662-keV gamma radiation arises from an isomeric transition of halflife 2·6 min in ^{137}Ba^m to the $\frac{3}{2}^+$ ground state. Use Fig. 9.4, correcting for the change in A-value, to confirm the spin of the isomeric state. Check from Fig. 9.8 that it was correct to use the observed halflife in making this deduction.

9.4* The isomeric state of ^{134}Cs^m (spin/parity 8^-) decays to the ground state (4^+) and to an excited state (5^+) by transitions of energy 137 and 127 keV. State the nature of the three transitions, and estimate the relative intensity of the 137- and 127-keV radiations.

9.5 Using the Weisskopf formulae (9.15) and (9.17) for a single-proton transition deduce an expression for the E3 radiative width.

9.6 The (upward) B(E2) value for the Coulomb excitation of the 2·938 MeV state (2^+) of ^{26}Mg is 40 e^2 fm^4. Calculate the radiative lifetime, if the branching ratio to the ground state is 10 per cent. [5×10^{-14} s]

9.7 In an experiment to determine the lifetime of an excited nucleus by the recoil-distance plunger method, the counting rate was found to decrease by a factor of 2 for a source displacement of 0·07 mm. If the mean lifetime of the decaying state is 7×10^{-11} s find the velocity of recoil. [$1{\cdot}4\times10^6$ m s^{-1}]

9.8 Ions of ^{32}S of energy 150 MeV were used to excite ^{64}Zn nuclei in order to measure an excited state lifetime by the plunger technique. When the plunger was 20 mm from the target 30 per cent of detected γ-rays were seen in the Doppler-shifted peak. Assuming that detection was in coincidence with back-scattered ^{32}S-ions, calculate the lifetime of the state. [$1{\cdot}9\times10^{-9}$ s]

9.9 Calculate the recoil velocity of the ^{59}Cu* nucleus formed in the ^{58}Ni (pγ) reaction at a proton energy of 3547 keV and the full Doppler shift expected for a gamma-ray of energy 3820 keV radiated by this nucleus. The energy of the gamma radiation actually observed is 3824 keV in the forward direction; what is the $F(\tau)$ value for use in a DSAM calculation? [$v = 0{\cdot}0015c$, 5·7 keV, 0.7]

9.10 Calculate the full recoil shift between the emission and absorption lines for the 411 keV level in ^{198}Hg, and the source velocity necessary to give complete overlap. [0·92 eV, 670 m s^{-1}]

9.11* In the experiment of Example 9·9, a resonance was also found at T_p = 1833 keV, and the DSAM lifetime was determined to be $1{\cdot}7\times10^{-14}$ s. If the proton width is 0·005 eV, and the spin of the resonant state is $\frac{5}{2}$, find the cross-section at resonance.

9.12 The 14·4-keV γ-ray transition in ^{57}Fe has been extensively studied using the Mössbauer effect, (e.g. Hanna *et al.*, *Phys. Rev. Letters* **4,** 177, 1960) and it is found that the $I=\frac{1}{2}$ ground state is split with an energy difference corresponding with a source velocity of 3·96 mm s^{-1}. If the ground-state magnetic moment is 0·0955 μ_N calculate the internal magnetic field at the ^{57}Fe nucleus. [31·5 T]

9.13 A nucleus X emits a beta particle forming a residual nucleus Y in an excited state of energy 250 keV. What is the minimum energy of the beta transition necessary to permit the gamma radiation from Y to be absorbed resonantly in an external nucleus Y at rest? [0.56 MeV]